

## Magnetic and Dielectric Properties of LiFePO<sub>4</sub>

Jae Yeon Seo, Hyunkyung Choi, Jung Tae Lim, and Chul Sung Kim\*

*Department of Physics, Kookmin University, Seoul 02707, South Korea*

(Received 3 July 2018, Received in final form 14 January 2019, Accepted 20 February 2019)

A LiFePO<sub>4</sub> was prepared using the ball milling. The X-ray diffraction patterns of the sample were measured, and the results confirmed that the sample's structure was orthorhombic with space group *Pnma*. The particle size and morphology of the sample prepared by the ball mill method confirmed by FE-SEM. The magnetization curves of the sample were measured using a vibrating sample magnetometer at temperatures of 4.2 to 295 K at 1000 Oe. The Néel temperature ( $T_N$ ) and spin-reorientation temperature ( $T_S$ ) were found to be 51.5 and 25 K, respectively. We investigated the magnetic hyperfine interaction using Mössbauer spectrometry at various temperatures between 4.2 and 295 K. At temperatures below  $T_N$ , the Mössbauer spectra of the sample were exhibited eight absorption lines resulting from the magnetic dipole and electric quadrupole interaction. The Fe ions state of sample at all temperatures were found to be ferrous state (Fe<sup>2+</sup>) ions. Debye temperature ( $\theta_D$ ) of  $433 \pm 5$  K was obtained for the sample. The permeability and permittivity were obtained using a Network analyzer.

**Keywords :** Mössbauer, magnetic properties, ball mill method, Li-ion batteries

### 1. Introduction

Olivine-type LiFePO<sub>4</sub> is promising for use as the cathode in Li-ion batteries because it is a low-cost material with possible environmental friendliness in large-scale applications, intended to reduce the use of fossil fuels [1-4]. In recent years, various manufacturing methods and performance enhancement techniques have been extensively studied [5-11]. Synthesis by ball milling is simple and energy efficient and has already been used for successful synthesis of LiFePO<sub>4</sub>. The ball milling decreases the particle size, reducing the ionic transport length, improving the cathode performance, and enhancing reversibility of the lithium ion intercalation/deintercalation [12, 13].

The magnetic properties of materials made by ball milling have not been well characterized. Understanding their magnetic properties is very important because their magnetic structure and properties are strongly related to their electrochemical performance [14-16].

In this paper, the magnetic properties and crystal struc-

ture of LiFePO<sub>4</sub> cathode materials synthesized by ball milling were investigated by X-ray diffraction (XRD), vibrating sample magnetometry (VSM), Mössbauer analysis, and network analyzer (NA).

### 2. Experimental Details

LiFePO<sub>4</sub> was synthesized by ball milling. The starting materials were Li<sub>2</sub>CO<sub>3</sub> (99.99 %), FeC<sub>2</sub>O<sub>4</sub>·2H<sub>2</sub>O (99 %), and NH<sub>4</sub>H<sub>2</sub>PO<sub>4</sub> (98 %); these materials were mixed in a ratio of 0.5 : 1 : 1. The mixture was ground with a rotation speed of 500 rpm for 24 h with acetone under an air atmosphere at room temperature and then dried at 60 °C under vacuum for 24 h. The mixture was then calcined at 300 °C for 4 h under Ar flow and pelletized at 5000 N/cm<sup>2</sup>. These pellets were sintered at 700 °C for 10 h under Ar flow. The structural characteristics of the prepared sample were analyzed X-ray diffraction (XRD) using Cu-K $\alpha$  radiation ( $\lambda = 1.5406$  Å), and Rietveld refinement using the FULLPROF program.

In order to observe the particle size and morphology of the sample prepared by the ball mill method, FE-SEM was used. The temperature-dependence of the magnetization curve below 1000 Oe was examined between 4.2 and 295 K. In addition, the Mössbauer spectra were measured at various temperature from 4.2 to 295 K using a

©The Korean Magnetism Society. All rights reserved.

\*Corresponding author: Tel: +82-2-910-5121

Fax: +82-2-910-4728, e-mail: cskim@kookmin.ac.kr

This paper was presented at the ICAUMS2018, Jeju, Korea, June 3-7, 2018.

conventional spectrometer moving at constant acceleration with a <sup>57</sup>Co radiation source in a Rh matrix. A Network analyzer (Agilent E5071C) was used to obtain the permeability and permittivity from 100 MHz to 4 GHz. The synthesized powder was pressed into a toroidal ring (inner diameter: 3.14 mm, outer diameter: 6.53 mm) and sintered at 500 °C to measure the magnetic properties.

### 3. Results and Discussion

The XRD patterns of LiFePO<sub>4</sub> were experimentally measured and analyzed by Rietveld refinement using the FULLPROF program, confirmed that the impurities other than LiFePO<sub>4</sub> were not synthesized, as shown in Fig. 1. It was also in good agreement with the neutron diffraction measurements obtained with the high-resolution powder diffractometer (HRPD) [17]. From the refined XRD pattern, the structure of LiFePO<sub>4</sub> was determined to be orthorhombic with space group *Pnma*. The lattice constants were found to be  $a_0 = 10.325 \text{ \AA}$ ,  $b_0 = 6.004 \text{ \AA}$ ,  $c_0 = 4.690 \text{ \AA}$ , and  $V = 290.805 \text{ \AA}^3$ . The Bragg factors  $R_B$  and  $R_F$  were 4.47 % and 4.98 %, respectively and was confirmed

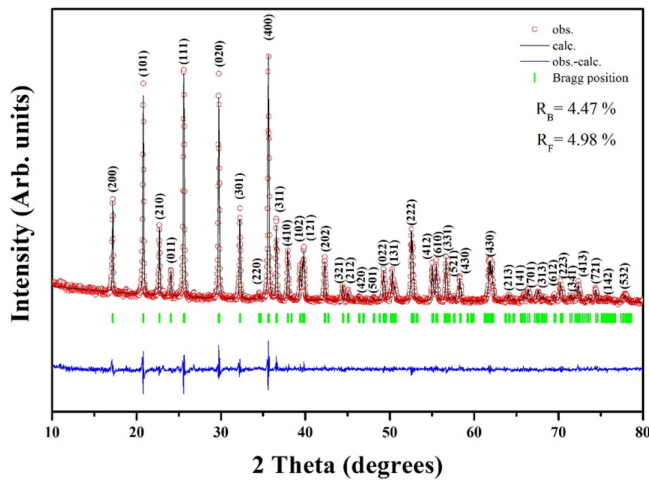


**Fig. 1.** (Color online) Refined XRD patterns of LiFePO<sub>4</sub> at room temperature.

**Table 1.** The coordinates of the O<sup>-</sup> ions in the FeO<sub>6</sub> Octahedral sites and the bond length between Fe-ion and six O-ions for LiFePO<sub>4</sub>.

Ions	$d_{\text{Fe-O}} (\text{\AA})$	Coordinates (x, y, z)
O <sub>1</sub>	2.192	(0.968, 0.250, 0.746)
O <sub>2</sub>	2.082	(0.452, 0.250, 1.213)
O <sub>3</sub>	2.255	(0.164, -0.430, 1.281)
O <sub>4</sub>	2.052	(0.335, -0.430, 0.781)
O <sub>5</sub>	2.052	(0.335, 0.543, 0.781)
O <sub>6</sub>	2.255	(0.164, 0.457, 1.281)

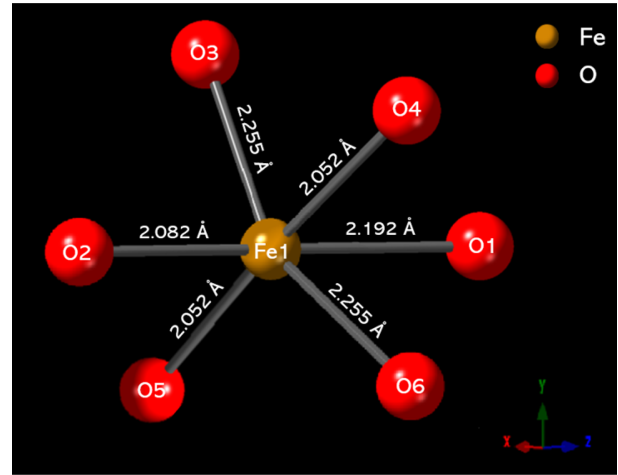


**Fig. 2.** (Color online) The Fe-O bond length between with FeO<sub>6</sub> octahedron for LiFePO<sub>4</sub>.

the crystal structure of single phase. The unit cell consists of four molecules, each of which contains LiO<sub>6</sub> octahedra running parallel to the *b*- axis, and of PO<sub>4</sub> tetrahedra, and

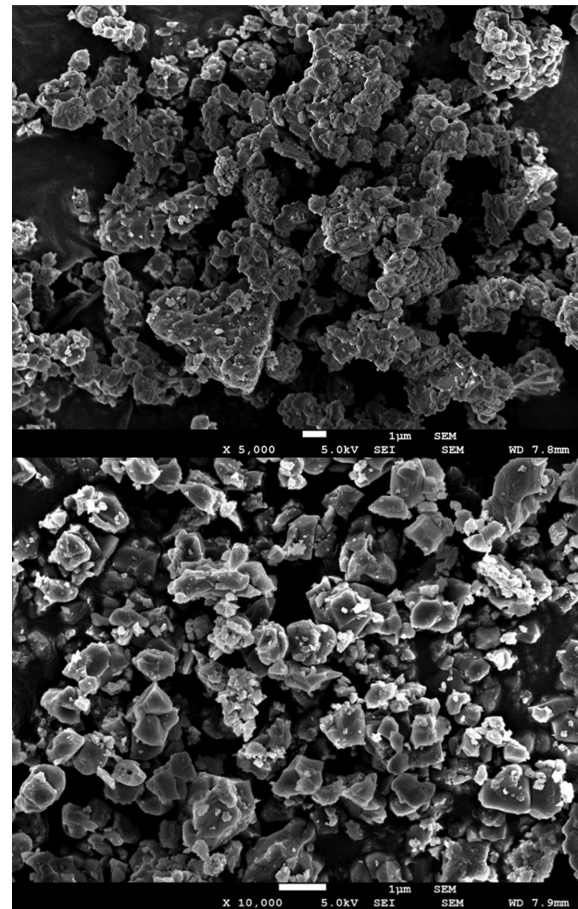


**Fig. 3.** FE-SEM images of LiFePO<sub>4</sub> prepared by the ball mill method.

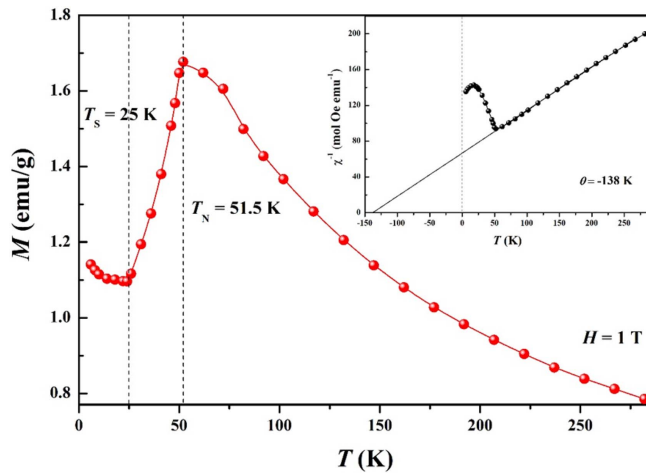


**Fig. 4.** (Color online) Temperature-dependent magnetization curve of the LiFePO<sub>4</sub> at various temperatures. The inset shows the inverse magnetic susceptibility  $\chi^{-1}(T)$  from the Curie-Weiss law fitting of the temperature-dependent curve.

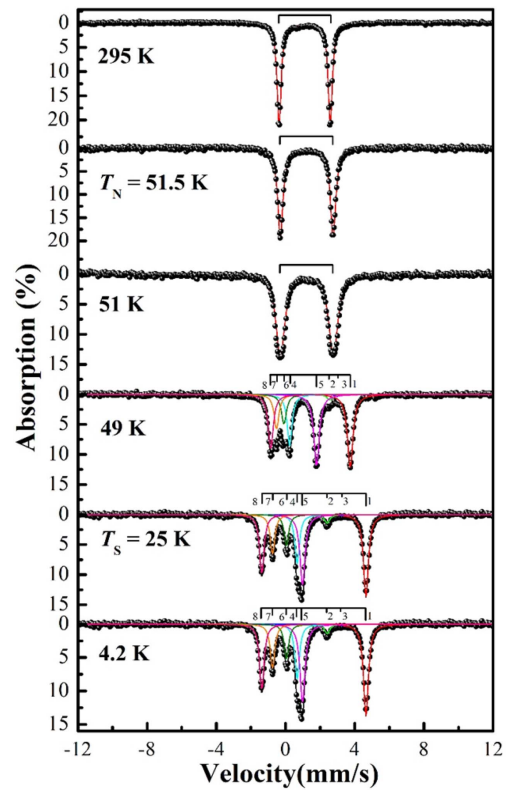
an asymmetric FeO<sub>6</sub> octahedral unit structure [17, 18].

Table 1 shows the coordinates of the O<sup>-</sup> ions in the FeO<sub>6</sub> octahedral sites as well as distances between the Fe<sup>2+</sup> ion and the six O<sup>-</sup> ions of LiFePO<sub>4</sub>, as shown in Fig. 2.

From the FE-SEM images, despite the high sintering process of 700 °C synthesized with the pure LiFePO<sub>4</sub> phase, the presence of particles with an average length, width, and thickness of approximately 0.5 to 1 μm is exhibited, as shown in Fig. 3.

To investigate the magnetic ordering, the temperature-dependent magnetization curves were obtained under an applied field of 1000 Oe, as shown in Fig. 4. The curves show typical antiferromagnetic (AFM) behavior at the magnetic Néel temperature ( $T_N$ ) of 51.5 K and a decrease in magnetization with decreasing temperature below  $T_N$ , the spin reorientation temperature ( $T_S$ ) was found to be 25 K. We fitted the curves to the modified Curie-Weiss law to obtain the inverse magnetic susceptibility  $\chi^{-1}(T)$  curve of LiFePO<sub>4</sub> at temperatures above  $T_N$ , as shown in the inset of Fig. 4. The obtained Curie-Weiss temperature is -138 K, indicating AFM ordering.

To investigate the Fe ions valence state of the Fe ions and the microscopic interaction mechanism between the quadrupole interaction and the hyperfine field in LiFePO<sub>4</sub>, Mössbauer spectra of the sample were obtained at various temperatures between 4.2 to 295 K. Figure 5 shows the temperature-dependent Mössbauer spectra of LiFePO<sub>4</sub>. At temperatures above  $T_N$ , the Mössbauer spectra have been analyzed with doublet. The Néel temperature ( $T_N$ ) was determined at 51.5 K, where the line width of the doublet was smaller than 51 K.



**Fig. 5.** (Color online) Mössbauer spectra of LiFePO<sub>4</sub> at various temperatures.

**Table 2.** Relative energies and intensities of the eight absorption lines in the Mössbauer spectrum of LiFePO<sub>4</sub> at 4.2 K.

Number	Position (mm/s)	Relative intensity
1	4.7038	6.91
2	2.3734	0.84
3	3.2222	0.09
4	0.7284	3.82
5	0.8919	6.16
6	0.0910	2.42
7	-0.7531	3.18
8	-1.3905	4.58

At temperatures below  $T_N$ , the Mössbauer spectra were analyzed by diagonalizing a  $4 \times 4$  magnetic dipole and electric quadrupole interaction matrix of the first excited state of a <sup>57</sup>Fe nucleus and fitting eight Lorentzian. The positions and intensities of the eight absorption lines are listed in Table 2. The following values at 4.2 K were obtained: magnetic hyperfine field ( $H_{hf}$ ) = 124.97 kOe, quadrupole splitting ( $\Delta E_Q$ ) = 2.74 mm/s, and isomer shift ( $\delta$ ) = 1.23 mm/s; the polar angle ( $\theta$ ) and azimuthal angle ( $\varphi$ ), which are the angles between the direction of  $H_{hf}$  at the Fe nucleus and the principal axes of the electric field gradient tensor, were determined to be 0. The asymmetric parameter ( $\eta$ ) is 0.80, and the ratio ( $R$ ) of the electric

**Table 3.** Mössbauer parameters of LiFePO<sub>4</sub>: magnetic hyperfine field ( $H_{\text{hf}}$ ), electric quadrupole splitting ( $\Delta E_Q$ ), isomer shift ( $\delta$ ), polar angle ( $\theta$ ), azimuthal angle ( $\varphi$ ), asymmetric parameter ( $\eta$ ), and ratio of the electric quadrupole interaction to the magnetic dipole interaction ( $R$ ), width of the line ( $\Gamma$ ), respectively.

$T$ (K)	$H_{\text{hf}}$ (kOe)	$\Delta E_Q$ (mm/s)	$\delta$ (mm/s)	$\theta$ (°)	$\varphi$ (°)	$\eta$	$R$	$\Gamma$ (mm/s)
4.2	124.97	2.74	1.23	0.0	0.0	0.8	3.24	0.33
25	120.65	2.79	1.23	0.0	0.0	0.8	3.36	0.35
49	63.92	2.70	1.23	0.0	0.0	0.9	6.24	0.36
51	-	2.70	1.23	-	-	-	-	0.62
51.5	-	3.05	1.23	-	-	-	-	0.35
295	-	2.95	1.09	-	-	-	-	0.28

quadrupole interaction to magnetic dipole interaction is 3.24. These parameters at various temperatures are listed in Table 3.

Figure 6 shows the reduced magnetic hyperfine fields  $H_{\text{hf}}(T)/H_{\text{hf}}(0)$  for LiFePO<sub>4</sub> as a function of the reduced temperature,  $T/T_N$  ( $T_N = 51.5$  K). The solid circles and

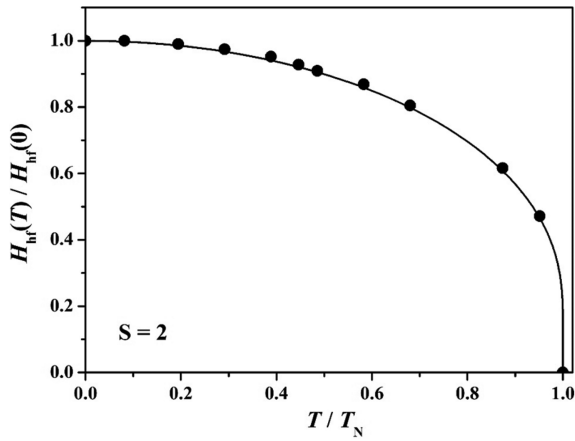


**Fig. 6.** Temperature-dependence of the magnetic hyperfine field ( $H_{\text{hf}}$ ) curve of LiFePO<sub>4</sub>. The inset shows enlarged plots of the magnetic hyperfine field at low temperature.

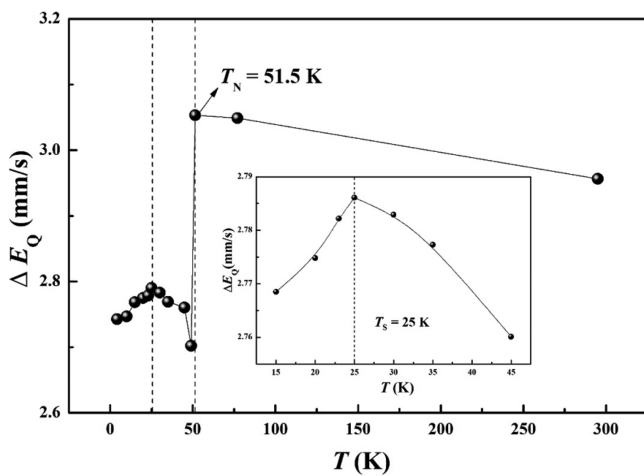


**Fig. 7.** Temperature-dependent electric quadrupole splitting ( $\Delta E_Q$ ) curve of LiFePO<sub>4</sub>. The inset shows a rapid change in the slope of the  $\Delta E_Q$  curve.

line represent the experimental data and the reduced Brillouin function for  $S = 2$ , respectively. From Brillouin functional analysis, we can obtain a spin value for the Fe ions of  $S = 2$  with only the spin contribution from the zero-orbital moment. Therefore, a spin value of  $S = 2$  without any orbital angular momentum is in good agreement with the Brillouin functional analysis of the Mössbauer spectroscopy data. From the reduced magnetic hyperfine field,  $H_{\text{hf}}(T)/H_{\text{hf}}(0)$  for LiFePO<sub>4</sub>, the spin value is determined to be  $S = 2$  [19, 20].

Figure 7 shows the curve of the temperature-dependent of electric quadrupole splitting ( $\Delta E_Q$ ) curve of LiFePO<sub>4</sub>. The slope of the temperature-dependent  $\Delta E_Q$  curves rapidly changes in spin-reorientation of each FeO<sub>6</sub> octahedron by the strong crystalline field below 25 K, as shown in the inset of Fig. 7. At temperatures above  $T_s$ ,  $\Delta E_Q$  decreases with increasing temperature due to spin-orbit coupling, which explained with only thermal contribution. From these results, we confirmed that the orbital angular momentum of the Fe<sup>2+</sup> ion is quenched by the strong crystalline field at temperatures above 25 K whereas the orbital angular moment contribution is enhanced at temperatures below 25 K due to the spin-orbit coupling effect [21].

Figure 8 shows the temperature dependence of the isomer shift ( $\delta$ ) for LiFePO<sub>4</sub>. The value of  $\delta$  depends on

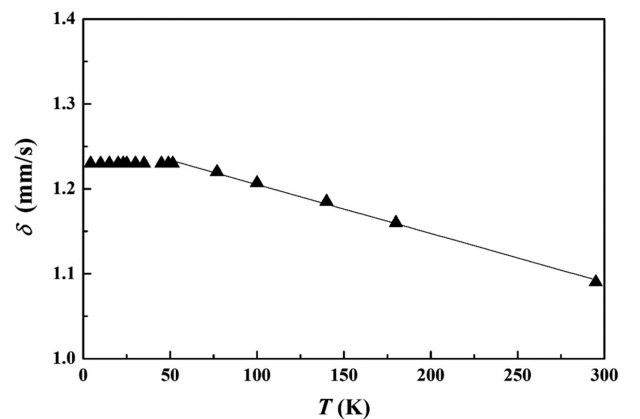


**Fig. 8.** Temperature dependence of isomer shift ( $\delta$ ) values for LiFePO<sub>4</sub>.

the electron charge density and is given by [22, 23]

$$\delta = \alpha[\rho_A(0) - \rho_S(0)], \quad (1)$$

where,  $\alpha$  is a negative number,  $\rho_A(0)$  and  $\rho_S(0)$  are the electron charge densities at the nuclear positions of the absorber (A) and source (S), respectively. The reason for this distinction is that even atoms of the same type can form different materials in gamma-ray sources and absorbers. The variable  $Ze$  is the nuclear charge, and  $r$  is the nuclear radius. The charge state of the Fe ions is ferrous ( $\text{Fe}^{2+}$ ) indicated from isomer shift ( $\delta$ ) value of between 1.09 and 1.23 mm/s at entire temperature range. The slope of the isomer shift value from Fig. 8. was calculated to be  $-0.0007$  mm/s·K, which corresponds to the theoretical value for  $^{57}\text{Fe}$ .

The Debye model gives the following expression for the recoil-free fraction [24, 25]

$$\ln f = -\frac{6E_R}{K_B\theta} \left( \frac{1}{4} + \frac{T^2}{\theta^2} \int_0^{\theta/T} \frac{tdt}{e^t - 1} \right), \quad (2)$$

where  $E_R$  is the recoil energy of  $^{57}\text{Fe}$  for the 14.4 keV gamma ray and  $\theta$  represents the Debye temperature.  $\ln f$  is plotted as a function of  $T^2$ , one obtains a curve that becomes almost linear in temperature. Mössbauer resonant absorption areas are proportional to the recoil-free fraction  $f$ , we fitted Eq. (2) with a proper additive constant was data in Fig. 9 using a least-squares computer program to obtain the Debye temperature of  $\theta_D = 433 \pm 5$  K.

Figure 10 shows the frequency dependence of the permittivity ( $\epsilon'$ ) and permeability ( $\mu'$ ) of  $\text{LiFePO}_4$  between 50 MHz and 4 GHz. The real part of the permittivity remains almost constant up to 4 GHz at  $4 < \epsilon' < 4.3$  and decreases with increasing frequency. The real part of the permeability is maintained at  $0.9 < \mu' < 1.3$  and decreases with increasing frequency.

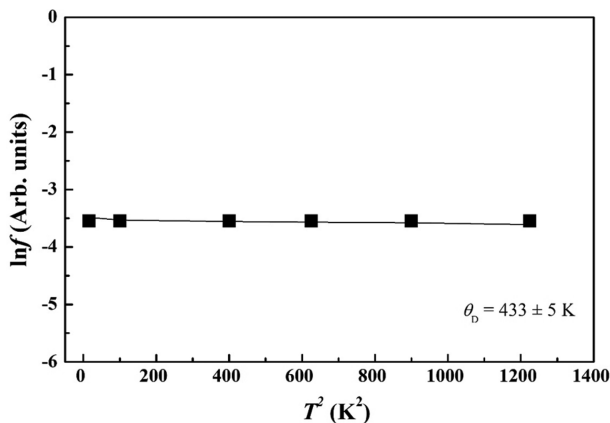


**Fig. 9.** Natural logarithm of the Mössbauer absorption area  $f$  vs  $T^2$  at low temperatures.

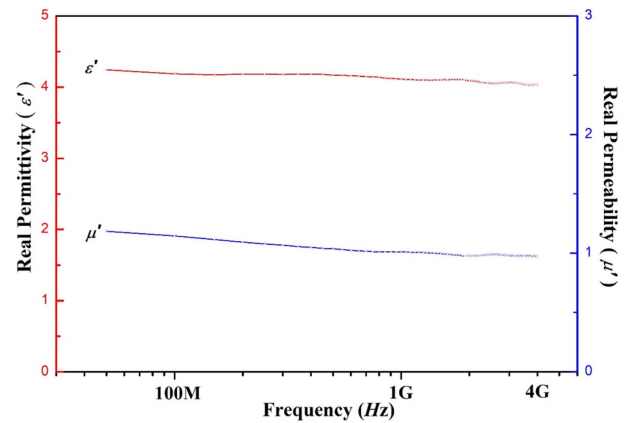


**Fig. 10.** (Color online) Real parts of the permittivity ( $\epsilon'$ ) and permeability ( $\mu'$ ) of  $\text{LiFePO}_4$  from the frequency dependent curves.

## 4. Conclusion

In summary, a  $\text{LiFePO}_4$  sample was successfully synthesized by the ball milling. We analyzed the crystal structure of the  $\text{LiFePO}_4$  was determined to be orthorhombic with space group  $Pnma$ , from XRD analysis. The strong crystalline field from the asymmetric Fe-O links affects the ferrous ( $\text{Fe}^{2+}$ ) ion. From the FE-SEM image, the particle size of  $\text{LiFePO}_4$  prepared by the ball mill method was confirmed to be about 0.5 to 1  $\mu\text{m}$ . From VSM measurements at various temperatures, we confirmed a decrease in the magnetization with decreasing temperature at temperatures below  $T_N = 51.5$  K, observed a typical AFM transition at  $T_N$ . The Curie-Weiss temperature obtained from the curve of the inverse susceptibility  $\chi^{-1}(T)$  is  $-138$  K, indicates the AFM ordering. In the Mössbauer spectra, the  $\text{Fe}^{2+}$  ion in  $\text{LiFePO}_4$  exhibits one set of the eight absorption lines at AFM regions were transformed into one set of the doublet at  $T_N = 51.5$  K. These results show the irregular spin arrangement with paramagnetic behavior due to thermal agitation at above  $T_N$ . The slope of  $H_{\text{hf}}$  and  $\Delta E_Q$  curves rapidly changed at  $T_s = 25$  K. This indicates that the abrupt change in the slope of  $H_{\text{hf}}$  and  $\Delta E_Q$  were caused by orbital angular momentum contribution of  $\text{Fe}^{2+}$  ion from the spin-orbit coupling. The calculated Debye temperature of the  $\text{LiFePO}_4$  was  $\theta_D = 433 \pm 5$  K. From the frequency-dependence curves, the real parts of the permittivity ( $\epsilon$ ) and permeability ( $\mu$ ) were found to decrease with increasing frequency.

## Acknowledgments

This work was supported by Mid-Career Researcher Program, through the National Research Foundation of

Korea (NRF), with a grant funded by the Ministry of Education, Science and Technology (MEST) (NRF-2017R1A2B2012241).

## References

- [1] A. Yamada, H. Koizumi, S. Nishimura, N. Sonoyama, R. Kanno, M. Yonemura, T. Nakamura, and Y. Kobayashi, *Nat. Mater.* **5**, 357 (2006).
- [2] T. Maxisch and G. Ceder, *Phys. Rev. B* **73**, 174112 (2006).
- [3] L. X. Yuan, Z. H. Wang, W. X. Zhang, X. L. Hu, J. T. Chen, Y. H. Huang, and J. B. Goodenough, *Energy Environ. Sci.* **4**, 269 (2011).
- [4] W. J. Zhang, *J. Power Sources* **196**, 2962 (2011).
- [5] K. Zaghbi, J. Dubé, A. Dallaire, K. Galoustov, A. Guerfi, M. Ramanathan, J. Prakash, A. Mauger, C. M. Julien, and A. Benmayza, *J. Power Sources* **219**, 36 (2012).
- [6] S. Deng, H. Wang, H. Liu, J. Liu, and H. Yan, *Nano-Micro Lett.* **6**, 209 (2014).
- [7] Y. Liang, K. Wen, Y. Mao, Z. Liu, G. Zhu, F. Yang, and W. He, *Chem. Electro. Chem.* **2**, 1227 (2015).
- [8] T. Wu, X. Ma, X. Liu, G. Zeng, and W. Xiao, *Mater. Technol.* **30**, 25 (2015).
- [9] Z. Xu, L. Gao, Y. Liu, and L. Li, *J. Electrochem. Soc.* **163**, A2600 (2016).
- [10] J. H. Seo, K. Verlinde, J. Guo, D. S. B. Heidary, R. Rajagopalan, T. E. Mallouk, and C. A. Randall, *Scripta Mater.* **146**, 267 (2018).
- [11] K. Zaghbi, A. Mauger, J. B. Goodenough, F. Gendron, and C. M. Julien, *Chem. Mater.* **19**, 3740 (2007).
- [12] G. T. K. Fey, Y. G. Chen, and H. M. Kao, *J. Power Sources* **189**, 169 (2009).
- [13] D. T. O'Connor, M. J. Welland, W. K. Liu, and P. W. Voorhees, *Modell. Simul. Mater. Sci. Eng.* **24**, 17 (2016).
- [14] J. Yao, K. Konstantinov, G. X. Wang, and H. K. Liu, *J. Solid State Electrochem.* **11**, 177 (2007).
- [15] S. J. Moon and C. S. Kim, *J. Korean Phys. Soc.* **53**, 1589 (2008).
- [16] J. Molenda, A. Kulka, A. Milewska, W. Zając, and K. Świerczek, *Materials* **6**, 1656 (2013).
- [17] C. H. Rhee, I. K. Lee, S. J. Moon, S. J. Kim, and C. S. Kim, *J. Korean Phys. Soc.* **58**, 472 (2011).
- [18] G. Rousse, J. Rodriguez-Carvajal, S. Patoux, and C. Masquelier, *Chem. Mater.* **15**, 4082 (2003).
- [19] A. Yamada, S. C. Chung, and K. Hinokuma, *J. Electrochem. Soc.* **148**, A224 (2001).
- [20] C. M. Julien, A. A. Salah, A. Mauger, and F. Gendron, *Ionics* **12**, 21 (2006).
- [21] G. Liang, K. Park, J. Li, R. E. Benson, D. Vaknin, J. T. Markert, and M. C. Croft, *Phys. Rev. B* **77**, 064414 (2008).
- [22] P. Ravindran, R. Vidya, H. Fjellvåg, and A. Kjekshus, *Phys. Rev. B* **77**, 134448 (2008).
- [23] H. N. Ok, *Mössbauer Spectroscopy*, Minumsa, Seoul, (1983) pp 32-33.
- [24] R. L. Mössbauer and W. H. Wiedemann, *Zeitschrift für Physik* **159**, 33 (1960).
- [25] C. S. Kim, I. B. Shim, M. Y. Ha, H. Choi, and J. C. Sur, *J. Korean Phys. Soc.* **23**, 166 (1990).